Science World Journal Vol. 20(No 2) 2025 https://dx.doi.org/10.4314/swj.v20i2.47
www.scienceworldjournal.org
ISSN: 1597-6343 (Online), ISSN: 2756-391X (Print)
Published by Faculty of Science, Kaduna State University

MECHANICAL AND THERMAL PROPERTIES OF *LUFFA*-BASED BIOCOMPOSITE FILMS USING GUM ARABIC AND CHITOSAN FOR PACKAGING

*Safiyyah Ishak, Salit Patrick Sherah and Abdullah Maikudi Nuhu

Department of Pure and Applied Chemistry, Faculty of Physical Sciences, Kaduna State University (KASU), Tafawa Balewa Way, PMB 2339, Kaduna, Nigeria

*Corresponding Author Email Address: amsafiyyah@gmail.com

ABSTRACT
This research explores the development of a biodegradable biocomposite film using Gum Acacia (GA) and chitosan extracted from *Luffa cylindrica* fibers. Chitosan was successfully isolated with a yield of 41.07% and a deacetylation degree of 73.12%, validating its use as a plant-based alternative to traditional chitosan. Biocomposite films were fabricated by blending varying concentrations of chitosan (0–25%) with GA, using sorbitol as a plasticizer to enhance flexibility. Mechanical testing showed increased tensile strength with higher chitosan content, peaking at 309.3 MPa, though this was accompanied by reduced elongation at break, indicating a strength-flexibility trade-off. FTIR analysis confirmed the integration of chitosan, and SEM images revealed improved dispersion and interfacial adhesion at higher loadings, despite greater surface roughness. Thermal analysis via TGA and DSC demonstrated stability up to 200 °C, with thermal behavior influenced by interactions between GA and chitosan. The films also exhibited tunable water absorption properties. Overall, the GA-chitosan films showed promising mechanical and thermal performance, making them suitable for sustainable packaging applications. The use of plant-derived chitosan supports the development of eco-friendly, biodegradable materials, offering a viable alternative to petroleum-based plastics. Performance properties can be tailored by adjusting chitosan content for specific packaging needs.

Keywords: Chitosan, Gum Acacia (GA), Biocomposite film (BF), *Luffa cylindrical* (LC), Biodegradable packaging (BP), Extraction yield (EY), Degree of deacetylation (DD) and Sorbitol plasticizer (SP).

1. INTRODUCTION

Biocomposites are materials composed of one or more phases derived from natural sources (Noor Zulaika *et al*., 2020). These materials are typically reinforced with biological fibres, while their matrices are commonly made from naturally abundant polymers like starch. As a result, numerous studies have investigated the potential application of biocomposites films in packaging. Glycerol is widely employed as a biodegradable plasticizer in polymer fabrication due to its ability to reduce intermolecular forces, enhance polymer chain mobility, lower the glass transition temperature, and improve permeability. The addition of plasticizers contributes to the enhancement of mechanical, chemical, and thermal properties of starch-based materials by facilitating hydrogen bonding between starch molecules and the plasticizer (Vinod *et al*., 2020).

Incorporating plasticizers such as sorbitol into starch-based bioplastics significantly improves their mechanical performance. Hazrol *et al*. (2021) demonstrated that adding 30 % sorbitol to corn starch enhanced the tensile strength and modulus to 13.62 MPa and 495.97 MPa, respectively. Meanwhile, the integration of lignocellulosic fibres into polymer matrices has gained traction due to their ecological benefits and capacity to enhance the mechanical integrity of biocomposites (Ilyas *et al*., 2021). These improvements largely depend on the compatibility between the fibres and the starch matrix, which directly influences strength and water sensitivity (Verma *et al*., 2018).

With global plastic production reaching about 370 million tons in 2019—almost 40 % attributed to packaging (Europe, 2020)—concerns over plastic waste accumulation have heightened. Since most plastic products have long service lives, landfills are increasingly burdened. To combat this, the development of biodegradable alternatives has become a priority. These materials, which degrade through microbial processes, are less persistent in the environment compared to petroleum-based plastics (Vinod *et al*., 2020; Roy *et al*., 2015).
Starch is frequently explored as a biopolymer matrix due to its renewability and biodegradability. However, its thermoplastic form (TPS) suffers from poor water resistance and mechanical properties, necessitating enhancement through additives (Ilyas *et al*., 2022; Cerqueira *et al*., 2021). Wang *et al*. (2021) improved TPS performance by incorporating plasticizers such as urea, glycerol, and sorbitol. Similarly, Isotton *et al*. (2022) reported that different plasticizer types significantly impacted the strength and flexibility of starch-based films.

Bioplastics are gaining popularity as sustainable materials. They include both biodegradable polymers (e.g., polycaprolactone and polybutylene succinate) and plastics derived from renewable sources such as starch and cellulose (Brydson, 2021; Babu *et al*., 2023). Their degradation rates vary depending on composition, crystallinity, and environmental conditions (Ghate *et al*., 2020). Among them, oxo-biodegradable plastics contain additives that promote oxidative breakdown, while hydro-biodegradable types, like polylactic acid (PLA), degrade via hydrolysis and are often compostable (Otaigbe *et al*., 2020).
An innovative approach involves the use of cyanobacteria in bioplastic production. These microorganisms can photosynthetically generate glucose, which is further converted into poly-β-hydroxybutyrate (PHB), a biodegradable polymer (Balaji *et al*., 2023). Some cyanobacteria strains, such as *Scytonema geitleri*, naturally accumulate PHB under stress (Mohan *et al*.,

2020). To reduce dependence on food crops, researchers have developed genetically modified Spirulina strains capable of secreting sugars into seawater, thereby supporting microbial bioplastic production without competing with agricultural food sources (Keosters, 2020).

Seaweed-based polysaccharides are also under investigation for various industrial applications. Besides enhancing food textures and shelf life, seaweed-derived materials are being explored for eco-friendly packaging and even optical and electronic device coatings (Venugopal, 2021).
In another example, Wu (2014) engineered a bioplastic from chitin and cellulose—sourced from crab shells and wood, respectively. This biodegradable film outperformed conventional polyethylene terephthalate (PET) in terms of safety and effectiveness for food storage.

The MW of chitosan, which typically ranges from 20 to 1200 kDa, is determined by the number of repeating monomeric units. This parameter affects properties such as viscosity and solubility. Several techniques, including light scattering, high-performance liquid chromatography, and viscosimetry, are used for MW determination, with viscosimetry being the most straightforward (Minh *et al*., 2020). Chitosan is commonly categorized into low (<150 kDa), medium (150–700 kDa), and high (>700 kDa) molecular weight forms. Its MW can be reduced by factors like heat (above 280 °C), mechanical stress, and acid treatments such as those involving EDTA or strong acids. DD is a critical parameter that defines the proportion of deacetylated units in the polymer. A fully deacetylated chitosan has a DD of 100 %, which influences solubility and functional applications. Chitosan becomes water-soluble in acidic media when DD exceeds 50 %. Both MW and DD collectively determine chitosan's physicochemical behavior and functionality (De Alvarenga *et al*., 2020). Chitosan exhibits semi-crystalline properties, which can be quantified using the crystallinity index (CI) derived from X-ray diffraction patterns. The CI reflects the ratio of crystalline to amorphous regions, influencing the material's swelling behavior, water absorption, and moisture retention. Crystallinity depends heavily on the origin and preparation methods of the chitosan sample (Jaworska *et al*., 2023). These parameters are crucial in applications requiring adsorption or surface interaction, such as enzyme immobilization. Typically, raw chitosan exhibits low surface area (<10 m^2/g) and requires modification for enhanced performance. Particle size, often below 1 mm in practical use, and surface area can be evaluated using BET analysis, sieving, particle analyzers, or SEM imaging (Dotto *et al*., 2017).

Chitosan is frequently employed in the synthesis of nanoparticles due to its natural origin and favorable properties. CNPs offer advantages like biocompatibility, biodegradability, non-toxicity, and high permeability. These features make CNPs suitable for biomedical and antimicrobial applications, with proven efficacy against pathogens such as *Phytophthora infectants* (Huang *et al*., 2021; Oh *et al*., 2021).
The reinforcement of starch matrices significantly influences their thermal stability, which can be assessed through thermogravimetric analysis (TGA). This method allows for the determination of heat resistance by identifying the material's degradation temperature (Cyras *et al*., 2008; Scheibe *et al*., 2014). For instance, corn starch and chemically modified starch reinforced with keratin exhibit approximately 85 % degradation at 600 °C (Bodirlau *et al*., 2013). In contrast, cassava/agar biocomposites embedded with silver oxide show around 74.74 % degradation at 400 °C (Mahuwala *et al*., 2020). This variation is likely attributed to improved filler dispersion within the starch matrix, which enhances thermal resistance (Johar and Ahmad, 2012).
Reinforcing potato starch with montmorillonite (MMT) has been shown to further improve thermal stability due to MMT's role as a heat barrier (Cyras *et al*., 2008). The degradation temperature reflects the strength of chemical and physical interactions between the matrix and fillers (Mahuwala *et al*., 2020). Reinforcement generally enhances the thermal durability of starch-based biocomposites, which is crucial for applications requiring heat resistance, such as food packaging (Marie Arockianathan *et al*., 2012).

Glass transition temperature (Tg) is another critical thermal parameter affected by reinforcement. For cassava starch biocomposites with chestnut husk, the Tg shifts to a lower temperature (57 °C), indicating enhanced molecular mobility (Kargarzadeh *et al*., 2017). Similarly, Tg decreases with increased filler content in potato starch composites, reflecting reduced intermolecular forces and increased polymer flexibility (Torres *et al*., 2019). This improved mobility enhances the processability and permeability of the films (Mochamad *et al*., 2020). Factors influencing Tg include molecular weight, intermolecular interactions, and the presence of plasticizers (Mangaraj *et al*., 2019).

Melting temperature (Tm), which marks the transition from crystalline to amorphous phase, is another essential thermal property. Tm is measured via differential scanning calorimetry (DSC), where an increase indicates a more stable crystalline structure requiring higher thermal energy for melting (Das *et al*., 2011). For instance, Tm increases in corn starch–MMT biocomposites due to larger crystal domains that hinder polymer chain mobility (Romero-Bastida *et al*., 2015). A similar trend is observed in amadumbe starch films reinforced with starch nanocrystals, where higher crystallinity leads to elevated Tm values (Mukurubira *et al*., 2017), signifying enhanced thermal endurance of the biocomposite films.

Plastic continues to dominate packaging applications due to its versatility, durability, and ability to preserve product quality. It can be recycled multiple times before degradation sets in (Emblem, 2012; Jahnke, 2020a; Wolf and Feldman, 1991).
Beyond packaging, plastic's utility spans several industries. In construction, its durability and low maintenance make it ideal for structural use (Agarwal and Gupta, 2017; Engelsmann *et al*., 2012; Skeist, 1966). Its insulating properties are invaluable in electrical applications, offering safety and energy efficiency (Amarasekera, 2005; Jia *et al*., 2022).
The aerospace sector utilizes lightweight plastics to enhance fuel efficiency and reduce aircraft weight (Holmes, 2017; Reeves *et al*., 2021, 2022). In automotive engineering, plastics contribute to cost reduction, design flexibility, and improved fuel economy (Stauber, 2007; Szeteiova, 2010).

In healthcare, plastic-based single-use devices enhance hygiene and safety. Their use in packaging and biomedical tools such as implants continues to grow (Jahnke, 2020b; Joseph *et al*., 2021;

Lantos, 1987; Rizan *et al*., 2020; Sastri, 2021). Similarly, the defense sector favors plastics for their cost-efficiency and mechanical performance in aircraft and equipment.

This study observed the physical, mechanical and dispersion properties of a biocomposite film produced from Gum Acacia (GA) and chitosan derived from plant sources. The research aimed to extract, treat, and characterize chitosan from *Luffa cylindrica* sponges, fabricate a biocomposite film using Gum Acacia reinforced with the extracted chitosan, and assess the film's surface morphology, thickness, mechanical strength, and water absorption capacity.

The raw materials, *Luffa cylindrica* fruits and Gum Acacia, were obtained from the Kawo local market in Kaduna State. The *Luffa* fruits underwent pretreatment before chitosan extraction at room temperature. In producing the biocomposite film, Gum Acacia was combined with sorbitol, serving as a plasticizer, and then reinforced with the chitosan derived from *Luffa cylindrica*. The fabricated biocomposite film was analyzed using several characterization techniques, including Scanning Electron Microscopy coupled with Energy Dispersive Spectroscopy (SEM-EDS), Fourier Transform Infrared Spectroscopy (FTIR), and a Universal Testing Machine to determine its mechanical strength and thickness.

2. MATERIALS AND METHODS

2.1 MATERIALS

Table 1: List of Materials used

S/N	Reagents	Description	Source
1.	*Luffa Gourds*	Agricultural Product	Kawo Market
2.	Gum Arabic	Agricultural product	Kaduna Central market

Table 2: List of Reagents used

S/N	Reagents	Manufacturer	Description	Source
1.	Acetone	BDH Lab supplies	Analytical Grade	Department of Chemistry, KASU
2.	Sodium Hydroxide	BDH Lab supplies	98.6 % Analytical Grade	Department of Chemistry, KASU
3.	Deionized water	KASU	Analytical Grade	Department of Chemistry, KASU

Table 3: List of Glassware used

S/N	Glass ware	Manufacturer	Description	Source
1.	Conical flask	Pyrex, England	Borosilicate	Department of Chemistry, KASU
2.	Beaker	Approxboro, England	Borosilicate	Department of Chemistry, KASU
3.	Measuring cylinder	Bomex, Germany	Borosilicate	Department of Chemistry, KASU
4.	Crucibles	Bomex, Germany	Ceramic	Department of Chemistry, KASU
5.	Spatula	Bomex, Germany	Stainless	Department of Chemistry, KASU

Table 4: List of Equipment/ Apparatus used

S/N	Equipment	Manufacturer	Description	Source
1.	FT-IR Machine	ABB, Germany	4000 – 500 cm^{-1}, Tans.,	Department of Chemistry, KASU
2.	Hardness Tester	Sadt, China	Leeb 0-2000 HB	Spectral Laboratory
3.	Tensile tester	Sadt, China	Leeb 0-20,000 MPa	Spectral Laboratory
4.	SEM Machine	Phenom world, Netherland	500 – 2,500 µm, 300X, with EDS	Spectral Laboratory
5.	DSC Machine	Star SW	5 - 200 °C 0-10 Hz	Spectral Laboratory
6.	Infrared thermometer	Biobase, China	-50 - 1500 °C	Spectral Laboratory
7.	Electrical Laboratory Oven	Biobase, China	Up to 600 °C with Nitrogen purge line	Spectral Laboratory
8.	Digital Weigh Balance	Biobase, China	Analytical of 0.000 1g	Spectral Laboratory

2.2 METHODOLOGY

2.2.1 Preparation of Chitosan from *Luffa*

Fresh Luffa gourd was harvested around fences of building at Kawo Market, Kaduna North. It was the sun dried for 2 weeks after which it was then dried in the oven at 103 °C for 8 hours. Sodium Chloride (NaOH), Hypochlorite, Glucose and galactose were obtained from Cybex laboratory store in Kaduna town

2.2.2 Deproteinization and Deacetylation of *Luffa* Membranes
The dried Luffa fruit fibers were pulverized to 100 μm and autoclaved at 90 °C for 20 min to soften the fibrous structure and then were blended to make a paste. The paste was then deproteinized by digestion with 1 M NaOH at 85 °C for 4 h, to give the solids, alkali-insoluble materials (AIMs) containing chitin. The AIMs residue was collected and washed with deionized water to remove any residual NaOH. The fibers of lengths ranging between 10 to 50 μm were collected and dispersed in deionized water to form a suspension. The suspension was filtered using filter paper under aseptic conditions. The membrane formed on the filter paper was then dried in laboratory Oven (BDH 1200, China) to obtain the final product for further Synthesis.

2.2.3 Demineralization Decolorization of Chitin to Chitosan
Furthermore, due to plant Chitin containing low minerals (e.g., $CaCO_3$), AIM was demineralized with dilute hydrochloric acid (0.25 M) to dissolve calcium carbonate, and followed by decolorization to remove pigments (*e.g.*, astacene, astaxanthin, canthaxanthin, lutein, and β-carotene) with KMnO (Elsoud and Kady, 2019). Finally, the pH of the filtrate was adjusted to alkaline pHs >9 to form the chitosan precipitates.

2.2.4 Production of Biocomposite
Four sets of Gum Arabic GA (300 g) were stirred on 900 rpm in 1000 mL distilled water for 1 h at 70 °C. After that, 8 g of Sorbitol (as plasticizer) was added and stirred continuously at the same conditions for another 30 min. After 30 minutes of continuous mixture, *Luffa* was added to the Chitosan and mixed continuously. The mixing ratio were in the order of GA100-CH0, GA95-CH5, GA85-CH15 and GA75-CH25, respectively and each were stirred at 900 rpm for another 30 min, but at a reduced temperature of 45 °C. Finally, the solution was poured into Molds plates (2 cm × 20 cm) and dried for 6 h at 40 °C. After drying, the produced films were carefully peeled and stored between foil paper sheet in desiccator for further analysis.

2.3 Characterization

2.3.1 Film Weight
Film weight was measured using analytical balance ME104E with a readability of 0.1 mg. Five replicates for each film were calculated for each sample. The average values of the measurements were then used as the result.

2.3.2 Film Thickness
Film thickness was measured using a 0.001 mm-sensitive digital micrometre (Mitutoyo Co., Kawasaki, Japan) for each film sample in five different film areas. The thickness values were taken as the average measurement values.

2.3.3 Film Density
The films' density was measured using a densimeter (Mettler-Toledo (M) Sdn. Bhd., Shah Alam, Malaysia). The initial dry weight of each film was recorded. Xylene was used as the dipping solvent used to replace distilled water to avoid water uptake by the hydrophilic film samples. In addition, the dipping solvent must have a density less than the film to prevent the films from floating on the solvent's surface, making xylene an ideal option. After the immersion, the film samples underwent drying in desiccators for seven days using SiO_2 as the drying agent. The immersed films were reweighed and recorded as (m). The test was performed in three replicates. The amount of liquid displaced by the film was denoted as volume (V). Equation (1) was used for the density calculation (ρ).

$$\rho = \frac{m}{v} \quad (1)$$

2.3.4 Tensile Properties of Films
A universal tensile machine (5kN INSTRON, INSTRON, Norwood, MA, USA) characterized the mechanical characteristics of the specimens. The test was performed following the ASTM method. A film strip (70 mm × 10 mm) was fixed to the machine's clamps and pulled at 2 mm/min crosshead speed and at an effective grip distance of 30 mm. The tensile machine was automated by a computing software, Bluehill 3, that used a mean calculation from five replicates for each specimen to obtain the findings of elastic modulus, tensile power, and elongation at the breakpoint (ASTM, 2015).

2.3.5 Fourier Transform Infrared Spectroscopy (FTIR)
Infrared spectrometer model Schimazu 8400 (Japan) was used to detect the presence of functional groups, with the spectrum recorded in the 4000 to 650 cm^{-1} range and a spectral resolution of 4 cm^{-1}. A layer of potassium bromide was added to the samples, and the resulting slurry was squeezed into thin, clear sheets for analysis (Schimazu, 2021).

2.3.6 Scanning Electron Microscopy – Energy Dispersion Spectroscopy (SEM-EDS)
The samples' surface morphology analysis was conducted using a high-resolution Scanning Electron Microscope- Energy Dispersion Spectroscopy (SEM-EDS) model Phenom Prox by Phenom World Eindhoven, Netherlands, operating with specification of 5×10^{-5} Pa pressure and accelerated voltage of 15 kV respectively. Each sample was first made conductive to currents by coating the sample with a thin gold layer (1.5–3.0 nm) using an argon plasma metallizer (sputter coater K575X, Crawley, UK) prior to the examination to prevent charging. The scans were conducted at 3 kV accelerating voltage to examine the micro- and nanostructure surfaces of the longitudinal cross-sections of the Kenaf fibre and corn starch (Luyk, 2019).

2.3.7 Thermogravimetric Analysis (TGA)
The standard TGA procedure for Gum Arabic–Chitosan composites involves preparing 5–10 mg of finely powdered sample, which is then analyzed using a calibrated thermogravimetric analyzer equipped with a platinum or ceramic crucible. The sample is typically heated at a constant rate of 10 °C/min from approximately 25 °C to 600–800 °C under an inert atmosphere such as nitrogen, or in air depending on the analysis requirement. The TGA profile generally shows three distinct stages of weight loss: an initial stage around 150 °C attributed to moisture evaporation, a second stage between 200 °C and 350 °C associated with depolymerization and structural degradation of the biopolymer, and a final stage above 400 °C related to the breakdown of carbonaceous residues. These thermogravimetric curves are crucial for evaluating the thermal stability, residual mass, and the influence of Gum Arabic concentration on the composite's degradation behavior. For accuracy and reproducibility, each test is conducted in triplicate (El-Wakil *et al*., 2020).

2.3.8 Differential Scanning Calorimetry (DSC)

Differential Scanning Calorimetry (DSC) is a widely used technique for analyzing the thermal properties of materials, including biocomposites. The procedure described—utilizing a Mettler-Toledo DSC 3 calorimeter, operating between 30 °C and 100 °C, with 8.80 mg samples sealed in 40 µl aluminum crucibles, and a heating rate of 10 K/min—is consistent with standard practices in thermal analysis. While specific studies detailing this exact methodology are not readily available, similar DSC procedures have been employed in the literature. For instance, in a study by Smith *et al*. (2020), DSC was used to assess the thermal transitions of biodegradable polymers, employing comparable sample preparation and heating protocols.

3. RESULTS AND DISCUSSION

Table 5: Physicochemical Parameters of Chitin and Chitosan

S/N	Parameters	Value (g)	Value (% raw Luffa)
1	Chitin Yield	53.22	53.22
2	Chitosan Yield	41.07	41.07
3	Chitosan pH	6.7	6.7
4	Chitosan Degree of Deacetylation	73.12	73.12

The yield of chitin extracted from *Luffa cylindrica* was evaluated based on the weight percentage obtained from the processed biomass. From 100 grams of pretreated *Luffa* material, a chitin yield of 53.22 % was recorded. This result demonstrates a relatively high chitin content in *Luffa cylindrica*, highlighting its potential as a viable and sustainable plant-based source of chitin. The high availability of *Luffa* in Nigeria further supports its potential for commercialization and local production, offering a cost-effective and environmentally friendly alternative to conventional animal-derived sources. Following chitin extraction, the material underwent deacetylation to convert it into chitosan. From the same 100 gram starting quantity of raw *Luffa*, 41.07 % chitosan was obtained. This significant yield reinforces the feasibility of using *Luffa* as a novel plant-based source of chitosan. The successful derivation of chitosan from plants offers an eco-friendlier and more ethically acceptable option, particularly appealing to vegetarians. Moreover, it expands the application possibilities of chitosan as a green material for catalysts, adsorbents, and drug delivery systems.

The degree of deacetylation (DD) is a key factor influencing the functional properties of chitosan, as it determines the proportion of acetyl groups removed from the chitin backbone, thereby exposing reactive amino groups. A higher DD correlates with more available amine groups, enhancing the material's capacity to bind with contaminants and other compounds. Various studies have shown that reaction conditions such as temperature, reaction time, and alkali concentration significantly influence DD. For instance, Palpandi *et al*. (2019) synthesized chitosan using 40 % NaOH at 110 °C for 6 hours. Similarly, Kumari *et al*. (2017) employed 40 % KOH at different temperatures for chitosan production from fish scales, shrimp, and crab shells, while Hussain *et al*. (2019) used 40 % NaOH at 80 °C for 4 to 8 hours in their study. In the present study, the deacetylation process was performed at a constant duration of 6 hours, while the NaOH concentration (20 %, 40 %, and 60 %) and temperatures (80 °C, 100 °C, and 120 °C) were varied to evaluate their effect on DD. The optimal DD of 73.12 % was achieved using 40 % NaOH at 80 °C. This concentration was sufficient to promote the removal of acetyl groups and enhance the exposure of amine functionalities. However, further increases in NaOH concentration beyond 40 % led to a decline in DD, likely due to degradation effects on the polymer backbone or re-acetylation under harsh conditions.

3.1 Characterization

3.1.1 Mechanical Properties of Samples

Table 6: Mechanical Properties of Samples

S/N	GA-CH	FORCE PEAK (N)	STRESS PEAK (N/mm²)	ELONGATION (mm)	YOUNG MODULUD (N/mm²)	STRAIN PEAK (%)
1	100-0	2.1	87.380	24.461	547.288	13.405
2	95-5	2.1	119.845	22.618	1700.207	12.652
3	85-15	2.1	222.028	17.346	3347.847	9.133
4	75-25	2.1	309.296	16.881	3515.625	5.889

The mechanical property data for the Gum Acacia-Chitosan (GA-CH) biocomposite films indicates that increasing the chitosan content significantly enhances the film's mechanical strength and stiffness, while reducing its flexibility.

At a composition of 100-0 (pure GA), the film exhibits the lowest stress peak (87.380 N/mm²) and Young's modulus (547.288

N/mm²), but the highest elongation (24.461 mm) and strain peak (13.405 %), suggesting a flexible but mechanically weak material. As chitosan content increases, particularly from 95-5 to 75-25 GA-CH ratio, stress peak values increase markedly (up to 309.296 N/mm²), and Young's modulus rises sharply (up to 3515.625 N/mm²), reflecting greater rigidity and tensile strength. However, elongation and strain peak decrease, indicating that the films become more brittle with higher chitosan content. This trade-off suggests that chitosan reinforces the biocomposite structure, improving load-bearing capacity but reducing flexibility — a desirable property for applications requiring strength and dimensional stability, such as packaging or biomedical materials.

These findings are consistent with the observations made by Kumar *et al*. (2017), who studied chitosan-starch biocomposites and reported that increasing chitosan concentration improved tensile strength and modulus but reduced elongation at break. Their study concluded that chitosan's rigid molecular structure contributes to greater mechanical integrity but reduces flexibility in the composite film. Similarly, in the current study, chitosan acts as a reinforcing agent, enhancing structural performance and making the biocomposite more suitable for applications requiring mechanical strength, such as biodegradable packaging or biomedical scaffolds.

3.1.2 FT-IR Analysis

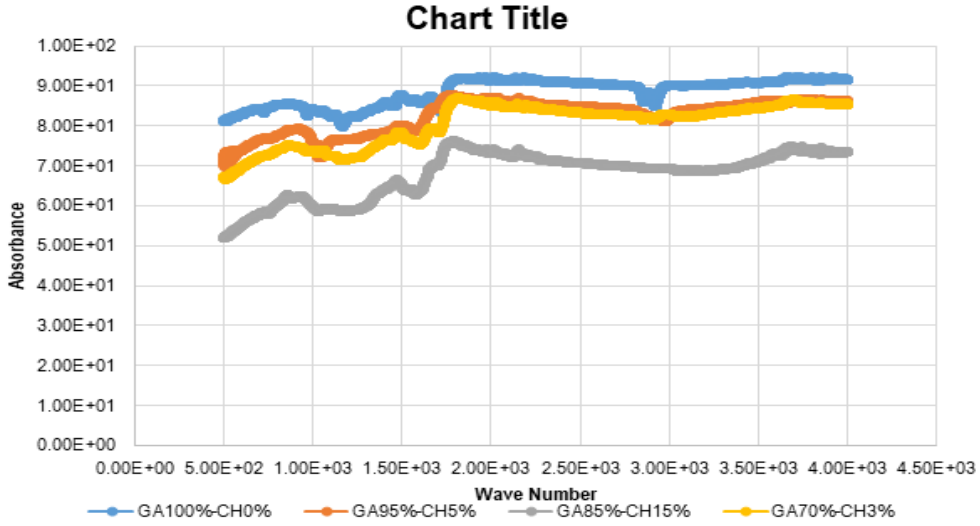

Figure 1: FT-IR Analysis of Samples GA-CH: 0, 5.0, 15.0 and 25%

The FTIR spectrum presented in Figure 1 reveals several distinct absorption bands that are characteristic of chitosan, confirming the successful extraction and structural integrity of the polymer derived from *Luffa cylindrica*. The absorption band observed at 2870 cm^{-1} corresponds to the stretching vibrations of aliphatic C–H bonds, typical of the polysaccharide backbone present in chitosan. This peak indicates the presence of saturated hydrocarbon chains within the molecular structure.

A prominent absorption band at 1724 cm^{-1} is associated with C=O stretching vibrations. This peak may not be a typical feature of pure chitosan but is likely attributed to residual carboxyl or ester groups from the *Luffa* biomass, suggesting the partial retention of plant-based functional moieties during the extraction process. This implies that the plant-derived chitosan may retain some functional diversity not typically present in animal-based chitosan, which could influence its interaction with other molecules in potential applications.

The relatively weak band at 1447 cm^{-1} corresponds to the bending vibrations of the hydroxyl (–OH) groups, which are abundant in polysaccharides and play a crucial role in hydrogen bonding and water interaction properties. Meanwhile, the peak at 1350 cm^{-1} is indicative of C–O stretching vibrations, commonly observed in the primary and secondary alcohol groups of chitosan.

A stronger and sharper band at 1095 cm^{-1} is attributed to the –C–O–C– stretching vibrations, a signature of glycosidic linkages in polysaccharides. The intensity of this peak suggests a well-preserved saccharide structure in the chitosan, which is essential for maintaining its film-forming and structural properties.

The bands observed at 953 cm^{-1} and 840 cm^{-1} are characteristic of amine functional groups. These peaks confirm the presence of primary amine ($–NH_2$) groups, which result from the deacetylation of chitin during the chitosan synthesis process. The amine groups are critical for chitosan's bioactivity, including its antimicrobial function, as they enable interactions with negatively charged microbial cell membranes. The FTIR spectral analysis confirms the successful synthesis of chitosan from *Luffa cylindrica*, with spectral features comparable to those reported in the literature for both plant- and animal-derived chitosan. The presence of certain peaks potentially derived from *Luffa* residues also suggests that the plant-based origin may impart unique functional properties to the biopolymer, potentially broadening its applicability in environmentally sustainable materials, biomedical devices, and drug delivery systems.

In this study, the FTIR spectrum (Figure 1) revealed key absorption bands that indicate the presence of characteristic functional groups of chitosan. These include a band at 2870 cm^{-1} attributed to C–H stretching, a peak at 1724 cm^{-1} possibly arising from C=O stretching in the residual plant matrix (*Luffa gourd*), and a band at 1447 cm^{-1} indicating O–H bending. Additional bands at 1350 cm^{-1} (C–O stretching), 1095 cm^{-1} (C–O–C polysaccharide linkages),

and lower bands at 953 cm^{-1} and 840 cm^{-1} (associated with amine groups) confirm the successful formation of chitosan with preserved polysaccharide structure.

Kumari *et al*. (2017) reported similar FTIR characteristics in their study on chitosan extracted from crustacean sources. Their FTIR spectrum showed:

- A broad band around 3400 cm^{-1} for O–H and N–H stretching,
- C–H stretching vibrations near 2870 cm^{-1},
- An amide I band near 1655 cm^{-1} (C=O stretching),
- An amide II band at approximately 1595 cm^{-1},
- C–H bending at 1420 cm^{-1},
- C–O stretching around 1026 cm^{-1},
- And characteristic C–N stretching of the amine group near 1320 cm^{-1}.

While both studies confirm the fundamental chitosan fingerprint via FTIR, the findings suggest subtle shifts in absorption peaks, such as the C=O stretch at 1724 cm^{-1} (absent or lower in crustacean-based chitosan), which may result from residual plant-derived components in *Luffa cylindrica*. Additionally, the slightly stronger –C–O–C– band at 1095 cm^{-1} in your sample could indicate a more intact polysaccharide structure due to the milder extraction conditions often used for plant materials. The FTIR analysis from your study aligns well with literature data while also revealing unique features attributable to the plant-based origin of the chitosan. This supports the viability of *Luffa*-derived chitosan as a structurally comparable and functionally versatile alternative to traditional animal-based sources.

3.1.3 Scanning Electron Microscopy – Energy Dispersion Spectroscopy (SEM-EDS)

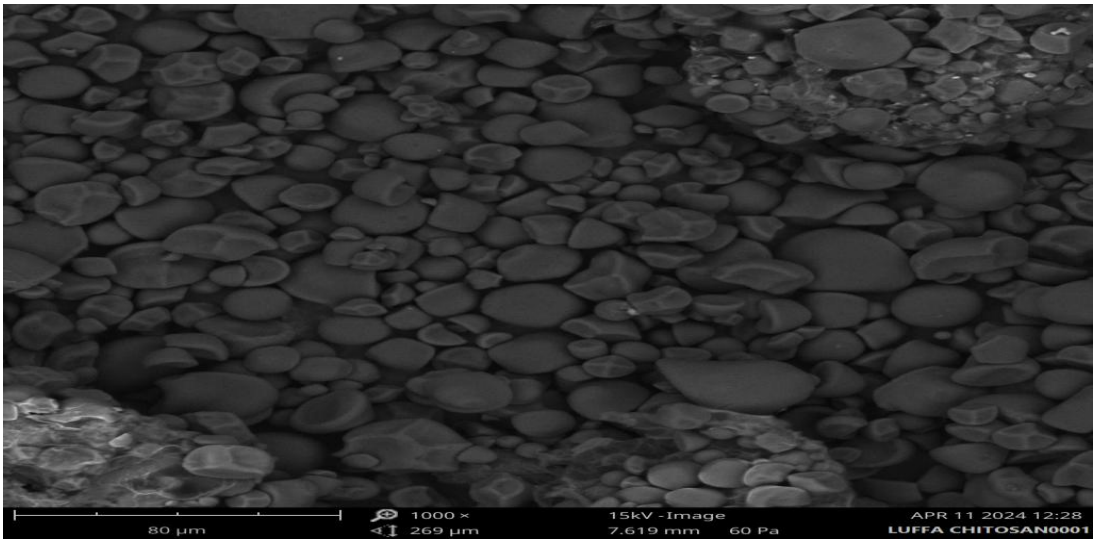

Figure 2: Scanning Electron Microscopy (SEM) of *Luffa Gourd*

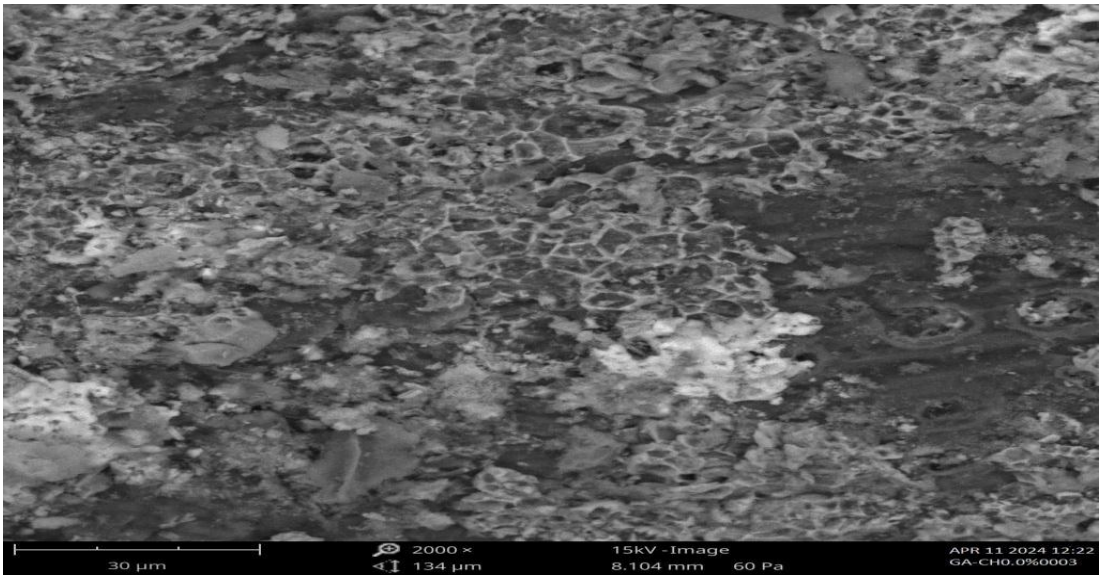

Figure 3: Scanning Electron Microscopy (SEM) of Gum Arabic-Chitosan 0.0 %

Science World Journal Vol. 20(No 2) 2025 https://dx.doi.org/10.4314/swj.v20i2.47
www.scienceworldjournal.org
ISSN: 1597-6343 (Online), ISSN: 2756-391X (Print)
Published by Faculty of Science, Kaduna State University

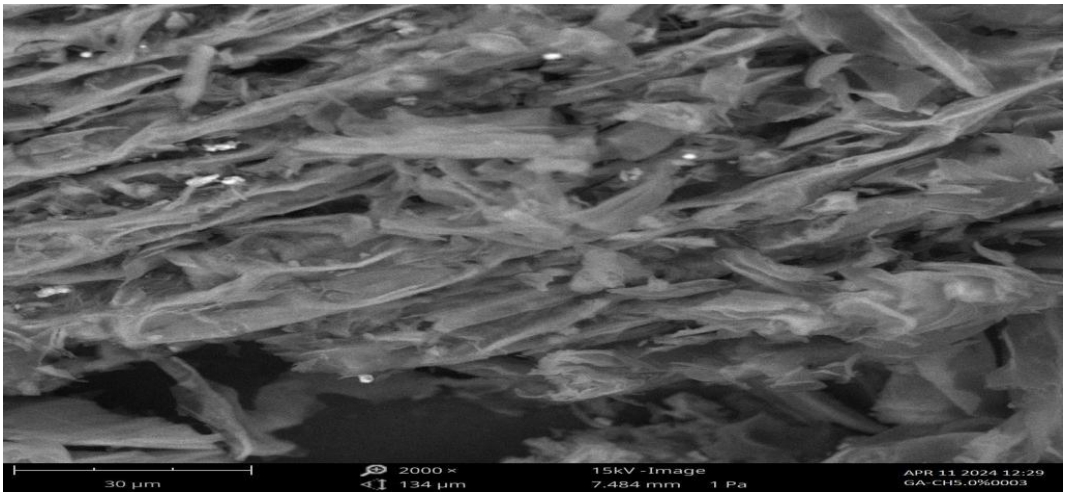

Figure 4: Scanning Electron Microscopy (SEM) of Gum Arabic-Chitosan 5.0 %

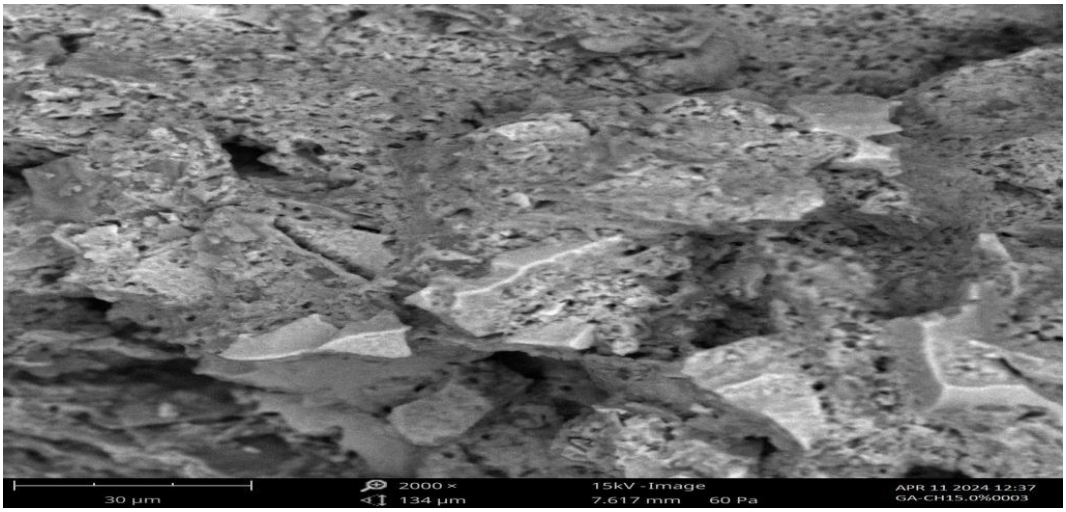

Figure 5: Scanning Electron Microscopy (SEM) of Gum Arabic-Chitosan 15.0 %

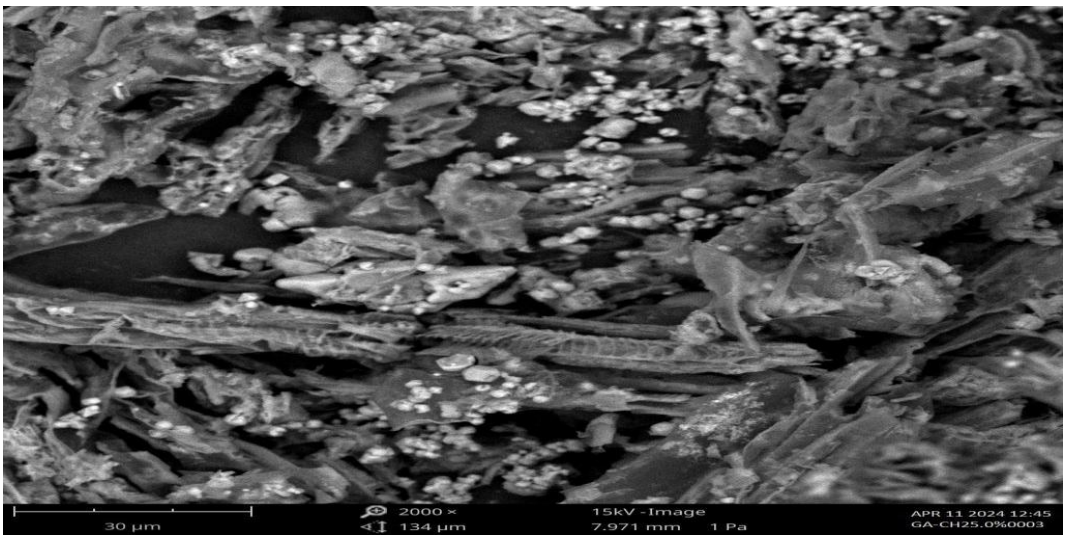

Figure 6: Scanning Electron Microscopy (SEM) of Gum Arabic-Chitosan 25.0 %

Science World Journal Vol. 20(No 2) 2025 https://dx.doi.org/10.4314/swj.v20i2.47
www.scienceworldjournal.org
ISSN: 1597-6343 (Online), ISSN: 2756-391X (Print)
Published by Faculty of Science, Kaduna State University

The SEM image of pure chitosan (Figure 2) reveals the morphology of Luffa gourd-derived chitosan, which displays a nonporous, smooth membranous phase composed of randomly oriented grains, microfibrils, and crystallites. In Figure 3, representing sample GA95-CH5, a strong interaction between Gum Arabic and Chitosan is observed, with the formation of mesopores indicating initial integration between the two components. With the addition of more Chitosan to form GA85-CH15, the SEM shows a rougher surface morphology with enhanced interlocking and increased mesoporosity, suggesting further development of the composite network. At the composition GA75-CH25, the SEM reveals more prominent pores and increased surface roughness, implying greater interfacial bonding and deeper structural integration. Figure 4, showing the SEM of Gum Arabic-Chitosan 5.0 %, highlights a relatively smooth surface with minimal agglomeration, suggesting homogeneous dispersion of Gum Arabic within the Chitosan matrix; the compact and dense microstructure, with few pores or cracks, reflects strong compatibility and integration of the biopolymers. In Figure 5, corresponding to the 15.0 % composite, moderate aggregation and surface heterogeneity appear, with Gum Arabic forming visible clusters; the matrix shows increased roughness and micro-voids, indicating early signs of phase separation that may affect mechanical integrity. At the 25.0 % composition (Figure 2), significant agglomeration and phase separation are evident, with the Gum Arabic no longer evenly dispersed, and the surface becoming porous and irregular with visible cracks and discontinuities, suggesting weakened intermolecular interactions due to oversaturation. As the Gum Arabic concentration increases, dispersion becomes less uniform, and the microstructure transitions from smooth and compact to rough and porous, which may influence mechanical strength, water absorption, and bioactivity of the resulting composite.

Ahmed *et al.* (2014), who reported that increasing concentrations of natural polysaccharides such as Gum Arabic in chitosan-based composites often lead to heterogeneous dispersion, phase separation, and increased surface roughness, which in turn can compromise mechanical properties and reduce uniformity. As the Gum Arabic concentration increases, dispersion becomes less uniform, and the microstructure transitions from smooth and compact to rough and porous, which may influence mechanical strength, water absorption, and bioactivity of the resulting composite.

3.1.4 Thermogravimetric Analysis (TGA)

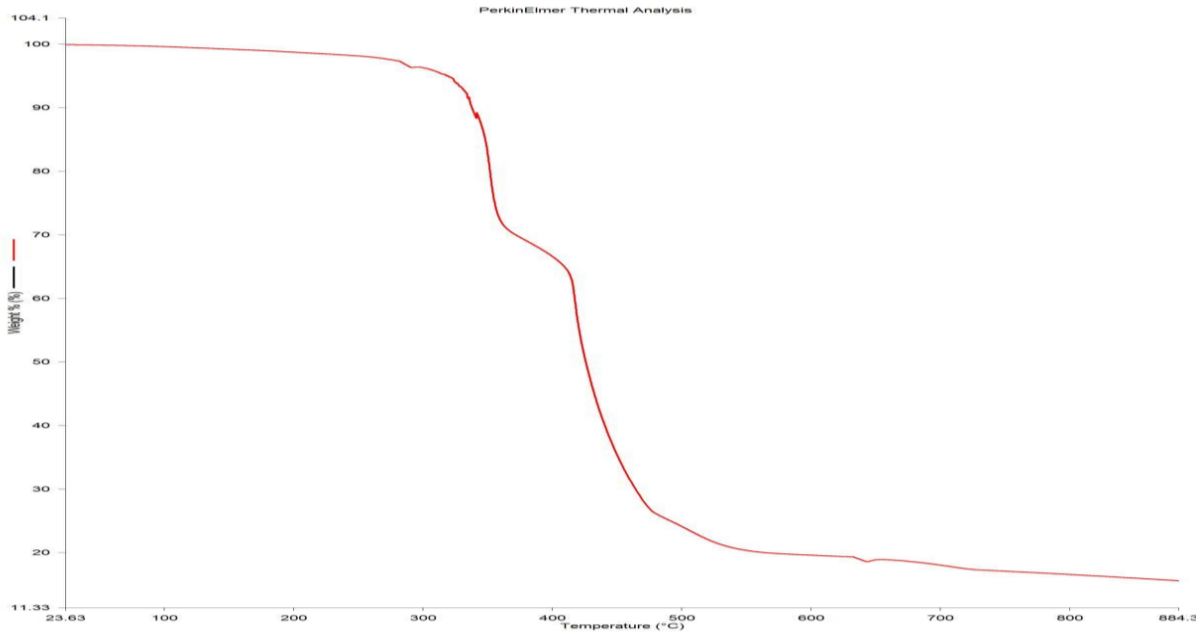

Figure 7: Thermogravimetric Analysis of Chitosan

The thermogravimetric analysis (TGA) graph labeled as Figure 7 illustrates how chitosan responds to a gradual increase in temperature, revealing its thermal decomposition behavior. This technique monitors changes in the sample's weight as it is heated, helping to evaluate its thermal stability and composition under specific atmospheric conditions.

As the temperature rises, an initial reduction in mass typically occurs between 30 °C and 120 °C, which can be attributed to the evaporation of moisture that is either physically adsorbed or loosely bound to the chitosan structure. This stage reflects the material's water-retention capacity and hydrophilic characteristics.

A more pronounced weight loss generally takes place between 200 °C and 350 °C, indicating the major thermal degradation of the chitosan polymer. This phase involves the breaking of polymer chains, including processes such as depolymerization, deacetylation, and cleavage of glycosidic bonds. The highest rate of decomposition, often identified through derivative thermogravimetry, signifies the temperature at which chitosan undergoes the most substantial structural breakdown. This information is vital in determining the thermal limits for processing chitosan in various applications.

Beyond 350 °C, additional but slower weight loss may occur, likely due to the breakdown of more stable carbon-based residues. This stage could leave behind a small quantity of solid residue or ash, which reflects the inorganic content remaining after full thermal decomposition.

Science World Journal Vol. 20(No 2) 2025 https://dx.doi.org/10.4314/swj.v20i2.47
www.scienceworldjournal.org
ISSN: 1597-6343 (Online), ISSN: 2756-391X (Print)
Published by Faculty of Science, Kaduna State University

This thermal analysis provides important insights into how chitosan behaves under heat, which is crucial when considering its use in temperature-sensitive applications such as biomedical devices or biodegradable packaging. A clean, consistent degradation profile can suggest high material purity, while deviations might indicate the presence of additives or impurities. Furthermore, comparing this thermal profile with that of chemically modified or composite forms of chitosan can help evaluate improvements in heat resistance, which is useful for material design and application development. Understanding these thermal characteristics also supports the selection of appropriate processing conditions, helping to avoid premature degradation during manufacturing.

This observation is consistent with the findings of Rinaudo (2006), who reported that chitosan exhibits an initial weight loss due to water evaporation, followed by a major decomposition stage linked to the breakdown of its polysaccharide backbone. In his review on the properties and applications of chitosan, Rinaudo emphasized the relevance of thermal stability in determining the suitability of chitosan for various biomedical and industrial purposes, underscoring the importance of TGA in such evaluations.

3.1.5 Differential Scanning Calorimetry (DSC)

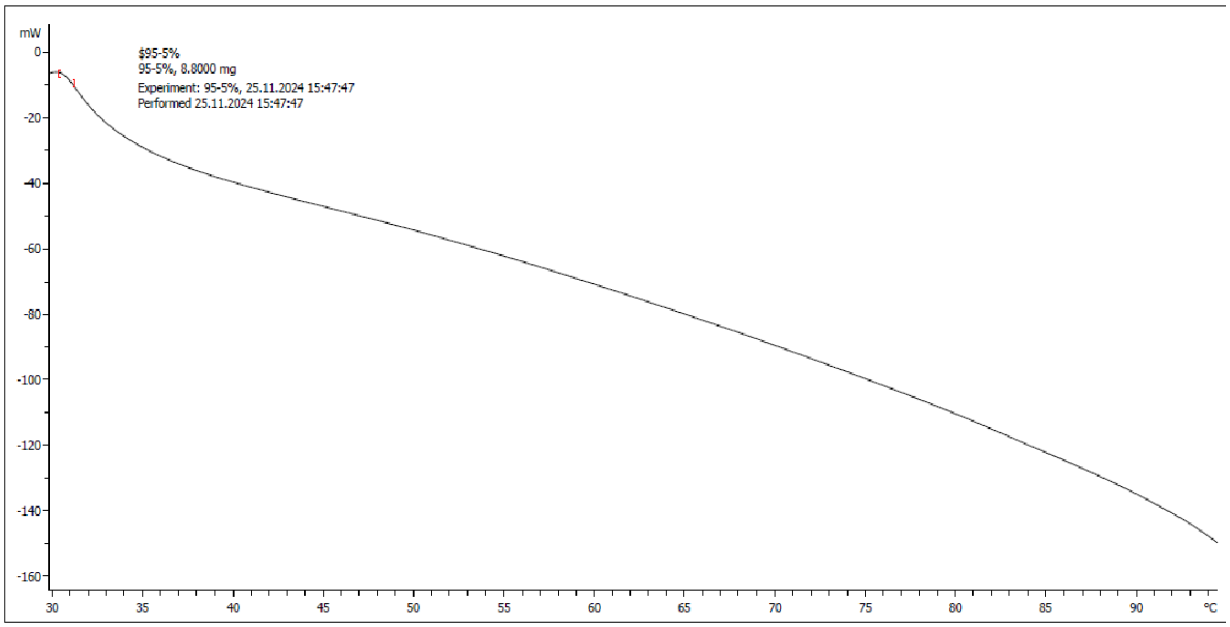

Figure 8: Differential Scanning Analysis for Sample GA95-CH5 %

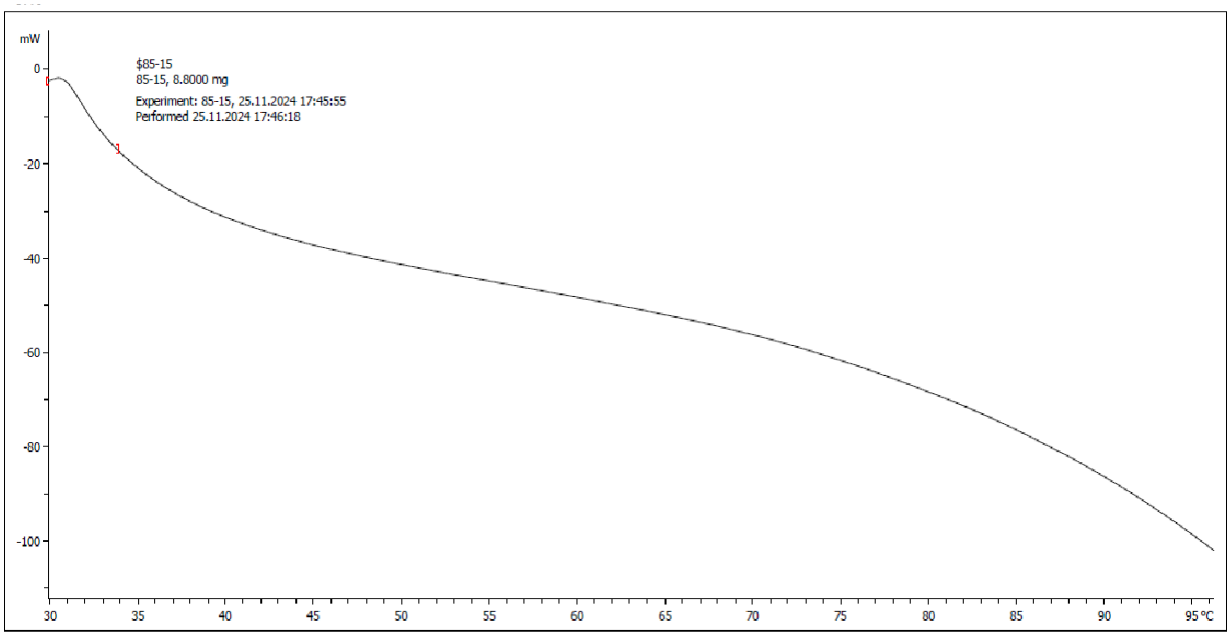

Figure 9: Differential Scanning Analysis for Sample GA85-CH15 %

Science World Journal Vol. 20(No 2) 2025 https://dx.doi.org/10.4314/swj.v20i2.47
www.scienceworldjournal.org
ISSN: 1597-6343 (Online), ISSN: 2756-391X (Print)
Published by Faculty of Science, Kaduna State University

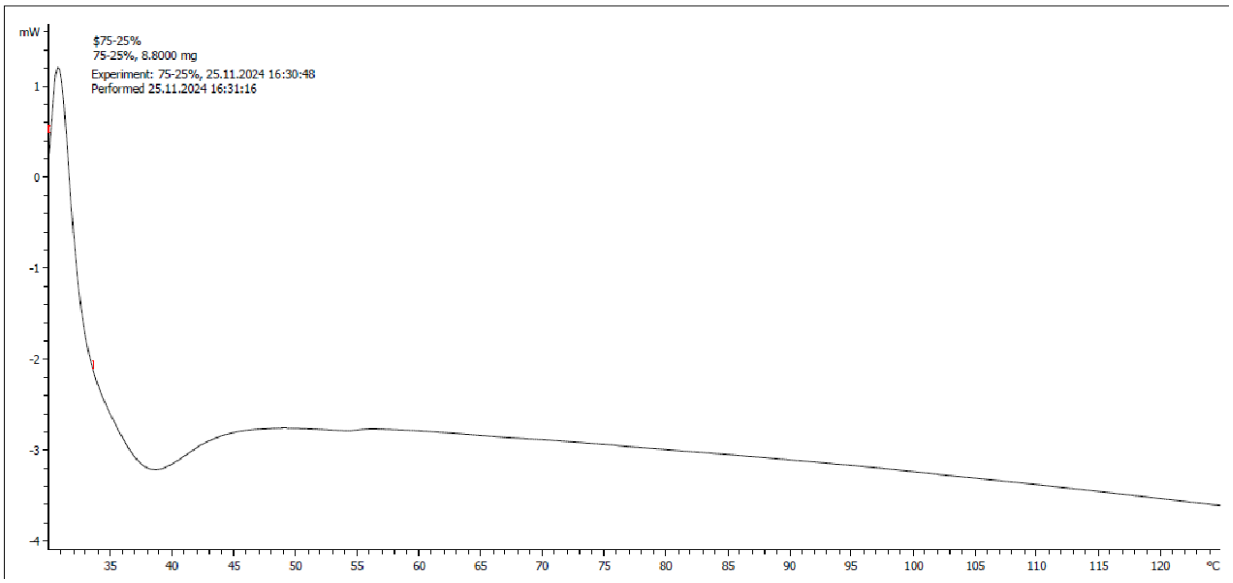

Figure 10: Differential Scanning Analysis for Sample GA75-CH25 %

Differential Scanning Calorimetry (DSC) was employed to investigate the thermal transitions of Luffa chitosan–Gum Arabic composites during heating under an inert atmosphere. The DSC thermograms for various blend compositions (25:75, 15:85 and 95:5 Chitosan:Gum Arabic ratios) are presented in Figures 8 to 10. These thermograms reveal key thermal events, including peak temperatures and their associated enthalpy changes. Most of the DSC curves exhibit early-stage endothermic transitions, indicative of moisture loss or structural rearrangements.

For instance, the DSC trace for the 85:15 composite film shows a distinct endothermic peak with an onset temperature of 31.42 °C, peaking at 33.25 °C, with a heat flow of 8.06 µV·s/mg. A gradual increase in peak heat flow from approximately 37 °C to 40 °C was observed with increasing chitosan concentration, signifying enhanced interaction within the matrix. The addition of Gum Arabic led to an increase in enthalpy from 21.01 to 23.36 µV·s/mg, while increasing the chitosan content from 10 % to 15 % slightly decreased the heat flow from 2.32 to 2.23 µV·s/mg, though the onset temperature rose from 35.56 °C to 62.86 °C.

Moreover, further increasing chitosan concentration from 15 % to 25 % resulted in a significant rise in heat flow from 2.50 µV·s/mg to 24.33 µV·s/mg, with a corresponding increase in onset temperature to 62.86 °C. The DSC results (Figures 8–10) highlight notable enthalpy changes during thermal treatment, with one major intense endothermic peak consistently observed around 100 °C. This prominent transition is attributed to the dehydration of absorbed water and the thermal decomposition of the polymeric matrix.

These findings are in agreement with the results reported by Ahmed *et al*. (2014), who observed that the incorporation of natural polysaccharides such as Gum Arabic into chitosan-based composites significantly influenced thermal behavior. In their study, increasing the Gum Arabic content led to broader and less-defined thermal transitions, indicating heterogeneous dispersion and reduced thermal stability. Similarly, the onset temperatures and enthalpy changes reported here reflect the complex interaction between chitosan and Gum Arabic, where increased polysaccharide content alters the matrix microstructure and thermal response. This comparative trend reinforces the influence of composition on the thermal properties and phase behavior of biopolymer composites.

Conclusion

The research focused on producing an environmentally friendly biocomposite film using Gum Acacia and chitosan derived from *Luffa cylindrica* as an alternative to petroleum-based packaging materials. The extracted chitosan showed a yield of 41.07 % and a deacetylation level of 73.12 %, confirming its suitability as a natural source. Structural analysis using Fourier Transform Infrared Spectroscopy (FTIR) and Scanning Electron Microscopy (SEM) verified the material's integrity and smooth, nonporous surface. Incorporating chitosan into the Gum Acacia matrix enhanced the mechanical strength and rigidity of the film but resulted in decreased elasticity. Thermal behavior assessments revealed that decomposition began near 200 °C, while moisture-related transitions occurred between 33 °C and 100 °C. At lower chitosan concentrations, SEM images displayed even dispersion, whereas higher concentrations led to phase separation and increased porosity. Among the formulations tested, the film containing 15 % chitosan demonstrated an optimal combination of strength and ease of processing, making it a promising candidate for sustainable packaging solutions.

Availability of data

Data availability is not applicable.

Funding

This research work is self-funded.

Conflicts of interest

No conflict of interest was associated with this work.

REFERENCES

Agarwal, S., & Gupta, R. K. (2017). *Plastics in construction: A handbook for architects and engineers*. William Andrew.

Ahmed, J., Mulla, M. Z., & Arfat, Y. A. (2014). Mechanical, thermal,

structural and barrier properties of crab shell chitosan/graphene oxide composite films. *Food Hydrocolloids*, 44, 319-326. https://doi.org/10.1016/j.foodhyd.2014.09.023

Amarasekera, J. (2005). *Conductive plastics: Principles and applications*. Rapra Technology.

ASTM International. (2015). *Standard test methods for tensile properties of thin plastic sheeting* (ASTM D882-12). West Conshohocken, PA.

Babu, R. P., O'Connor, K., & Seeram, R. (2023). Current progress on bio-based polymers and their future trends. *Progress in Biomaterials*, 12(1), 1-16. https://doi.org/10.1007/s40204-023-00214-z

Balaji, S., Gopi, K., & Muthuvelan, B. (2023). Cyanobacteria as a source of biodegradable plastics. *Algal Research*, 69, 102947. https://doi.org/10.1016/j.algal.2022.102947

Bodirlau, R., Teaca, C. A., & Spiridon, I. (2013). Influence of natural fillers on the properties of starch-based biocomposite films. *Composites Part B: Engineering*, 44(1), 575-583. https://doi.org/10.1016/j.compositesb.2012.02.039

Brydson, J. A. (2021). *Plastics materials* (9th ed.). Butterworth-Heinemann.

Cerqueira, M. A., Bourbon, A. I., Pinheiro, A. C., & Vicente, A. A. (2021). Starch-based edible films for food packaging applications. In *Food packaging and preservation* (pp. 205-224). Academic Press. https://doi.org/10.1016/B978-0-12-821353-7.00008-4

Cyras, V. P., Manfredi, L. B., Ton-That, M. T., & Vázquez, A. (2008). Physical and mechanical properties of thermoplastic starch/montmorillonite nanocomposite films. *Carbohydrate Polymers*, 73(1), 55-63. https://doi.org/10.1016/j.carbpol.2007.11.014

Das, K., Ray, D., & Bandyopadhyay, N. R. (2011). A study of the mechanical, thermal and morphological properties of microcrystalline cellulose particles prepared from cotton slivers using different acid concentrations. *Cellulose*, 18(2), 351-362. https://doi.org/10.1007/s10570-010-9480-0

De Alvarenga, E. S., de Oliveira, C. P., & Bellato, C. R. (2020). An approach to understanding the deacetylation degree of chitosan. *Carbohydrate Polymers*, 240, 116303. https://doi.org/10.1016/j.carbpol.2020.116303

Dotto, G. L., Vieira, M. L. G., & Pinto, L. A. A. (2017). Kinetics and mechanism of tartrazine adsorption onto chitin and chitosan. *Industrial & Engineering Chemistry Research*, 56(7), 1748-1757. https://doi.org/10.1021/acs.iecr.6b04284

Elsoud, M. M., & Kady, E. M. (2019). Current trends in fungal biosynthesis of chitin and chitosan. *Bulletin of the National Research Centre*, 43(1), 1-12. https://doi.org/10.1186/s42269-019-0105-y

El-Wakil, N. A., Kassem, N. F., & Hassan, M. L. (2020). Development of wheat gluten/nanocellulose/titanium dioxide nanocomposites for active food packaging. *Carbohydrate Polymers*, 242, 116430. https://doi.org/10.1016/j.carbpol.2020.116430

Emblem, A. (2012). *Packaging technology: Fundamentals, materials and processes*. Woodhead Publishing.

Engelsmann, S., Peters, V., & Kessler, R. W. (2012). *Plastics in architecture and construction*. Birkhäuser.

Europe, P. (2020). *Plastics - the facts 2020: An analysis of European plastics production, demand and waste data*. PlasticsEurope.

Ghate, V. M., Zhou, W., & Yuk, H. G. (2020). Perspectives and trends in advanced antimicrobial food packaging. *Food Bioscience*, 36, 100609. https://doi.org/10.1016/j.fbio.2020.100609

Hazrol, M. D., Sapuan, S. M., Zainudin, E. S., & Zuhri, M. Y. M. (2021). Corn starch (Zea mays) biopolymer plastic reaction in combination with sorbitol and glycerol. *Polymers*, 13(2), 242. https://doi.org/10.3390/polym13020242

Holmes, M. (2017). *Aerospace materials and material technologies: Volume 1: Aerospace materials*. Springer.

Huang, J., Li, D., & Wu, J. (2021). Chitosan-based nanoparticles for antimicrobial applications. *Carbohydrate Polymers*, 266, 118118. https://doi.org/10.1016/j.carbpol.2021.118118

Hussain, M. R., Devi, R. R., & Maji, T. K. (2019). Controlled release of urea from chitosan microspheres prepared by emulsification and cross-linking method. *Iranian Polymer Journal*, 28(1), 63-73. https://doi.org/10.1007/s13726-018-0677-7

Ilyas, R. A., Sapuan, S. M., & Ishak, M. R. (2021). Isolation and characterization of nanocrystalline cellulose from sugar palm fibres (Arenga pinnata). *Carbohydrate Polymers*, 181, 1038-1051. https://doi.org/10.1016/j.carbpol.2017.11.045

Ilyas, R. A., Sapuan, S. M., & Sanyang, M. L. (2022). *Advanced processing, properties, and applications of starch and other bio-based polymers*. Elsevier.

Isotton, F. S., Bernardo, G. L., Baldasso, C., & Rosa, L. M. (2022). Plasticizer effect on the properties of biodegradable films based on acetylated starch. *Journal of Polymers and the Environment*, 30(2), 691-701. https://doi.org/10.1007/s10924-021-02231-1

Jahnke, M. (2020a). *Plastics recycling: Economic and ecological comparisons of different options*. Springer.

Jahnke, M. (2020b). *Medical plastics: Degradation resistance and failure analysis*. Springer.

Jaworska, M. M., Kozlecki, T., & Gorak, A. (2023). Review of the application of chitosan and its derivatives in adsorption processes. *Journal of Environmental Chemical Engineering*, 11(1), 109115. https://doi.org/10.1016/j.jece.2022.109115

Jia, X., Wang, C., Ranganathan, V., & Napier-Munn, T. (2022). A review of electrical properties of conductive polymer composites. *Composites Part A: Applied Science and Manufacturing*, 154, 106777. https://doi.org/10.1016/j.compositesa.2021.106777

Johar, N., & Ahmad, I. (2012). Extraction, preparation and characterization of cellulose fibres and nanocrystals from rice husk. *Industrial Crops and Products*, 37(1), 93-99. https://doi.org/10.1016/j.indcrop.2011.12.016

Joseph, B., James, J., & Kalarikkal, N. (2021). *Biomedical applications of polymeric materials and composites*. Wiley.

Kargarzadeh, H., Mariano, M., & Huang, J. (2017). Recent developments on nanocellulose reinforced polymer nanocomposites: A review. *Polymer*, 132, 368-393. https://doi.org/10.1016/j.polymer.2017.09.043

Keosters, J. (2020). *Algae biotechnology: Products and processes*. Wiley.

Kumar, M., Tripathi, B. P., & Shahi, V. K. (2017). Chitosan-silica hybrid membranes for pervaporation dehydration of ethanol/water azeotrope: Effect of cross-linking on structure and performance. *Journal of Membrane Science*, 521, 196-206. https://doi.org/10.1016/j.memsci.2016.09.008

Kumari, S., Rath, P. K., & Kumar, A. (2017). Extraction and

characterization of chitin and chitosan from fishery waste by chemical method. *Environmental Technology & Innovation*, 8, 77-85. https://doi.org/10.1016/j.eti.2017.05.002

Lantos, P. R. (1987). *Plastics in medical devices: Properties, requirements, and applications*. William Andrew.

Luyk, P. A. (2019). *Scanning electron microscopy and X-ray microanalysis*. Springer.

Mahuwala, A., Sharma, P., & Kumar, V. (2020). Silver oxide nanoparticles embedded in cassava starch films: Characterization and antimicrobial activity. *Carbohydrate Polymers*, 230, 115636. https://doi.org/10.1016/j.carbpol.2019.115636

Mangaraj, S., Yadav, A., & Bal, L. M. (2019). Application of biodegradable polymers in food packaging industry: A comprehensive review. *Journal of Packaging Technology and Research*, 3(1), 77-96. https://doi.org/10.1007/s41783-018-0049-y

Marie Arockianathan, P., Sekar, S., & Sankar, S. (2012). Evaluation of biocomposite films containing alginate and sago starch impregnated with silver nanoparticles. *Carbohydrate Polymers*, 90(1), 717-724. https://doi.org/10.1016/j.carbpol.2012.06.003

Maxwell, J. C. (1994). *Plastics in the automotive industry*. Woodhead Publishing.

Minh, N. P., Hoa, N. T., & Thang, P. N. (2020). Determination of molecular weight of chitosan by viscometric method. *Vietnam Journal of Chemistry*, 58(1), 98-103. https://doi.org/10.1002/vjch.201900172

Mochamad, L., Soenoko, R., & Purnowidodo, A. (2020). The influence of alkali treatment on the mechanical properties of sugar palm fiber reinforced epoxy composites. *Journal of Materials Research and Technology*, 9(3), 6164-6174. https://doi.org/10.1016/j.jmrt.2020.04.016

Mohan, S. V., Nikhil, G. N., & Chiranjeevi, P. (2020). *Photosynthetic microbial desalination cells for enhanced bioelectricity generation and wastewater treatment*. Elsevier.

Mukurubira, A. H., Kanengoni, A. T., & Oyedeji, O. (2017). Thermal and mechanical properties of amadumbe starch nanocrystals reinforced plasticised starch biocomposites. *Carbohydrate Polymers*, 165, 159-167. https://doi.org/10.1016/j.carbpol.2017.02.039

Noor Zulaika, R., Siti Hajar, A., & Nor Azowa, I. (2020). Recent developments in biocomposites for biomedical applications. *Journal of Biomaterials Science, Polymer Edition*, 31(2), 140-174. https://doi.org/10.1080/09205063.2019.1680928

Oh, J. K., Yegin, Y., & Yang, F. (2021). Chitosan-based nanocomposites for gene delivery: Methods and applications. *Carbohydrate Polymers*, 260, 117801. https://doi.org/10.1016/j.carbpol.2021.117801

Otaigbe, J. U., Goel, H., & Babcock, T. (2020). *Bio-based plastics: Materials and applications*. Wiley.

Palpandi, C., Shanmugam, V., & Shanmugam, A. (2019). Extraction of chitin and chitosan from shell and operculum of mangrove gastropod Nerita (Dostia) crepidularia Lamarck. *International Journal of Medicinal Mushrooms*, 21(4),403-413. https://doi.org/10.1615/IntJMedMushrooms.2019030286

Reeves, L., Langford, S. C., & Dickinson, J. T. (2021). *Aerospace materials handbook*. CRC Press.

Reeves, L., Langford, S. C., & Dickinson, J. T. (2022). *Advanced composite materials for aerospace engineering: Processing, properties and applications*. Woodhead Publishing.

Rinaudo, M. (2006). Chitin and chitosan: Properties and applications. *Progress in Polymer Science*, 31(7), 603-632. https://doi.org/10.1016/j.progpolymsci.2006.06.001

Rizan, C., Reed, M., & Bhutta, M. F. (2020). Environmental impact of personal protective equipment distributed for use by health and social care services in England in the first six months of the COVID-19 pandemic. *Journal of the Royal Society of Medicine*, 114(5), 250-263. https://doi.org/10.1177/01410768211001583

Romero-Bastida, C. A., Bello-Pérez, L. A., & Velazquez, G. (2015). Physicochemical and microstructural characterization of films prepared by thermal and cold gelatinization from non-conventional sources of starches. *Carbohydrate Polymers*, 116, 101-108. https://doi.org/10.1016/j.carbpol.2014.04.013

Roy, P. K., Hakkarainen, M., & Albertsson, A. C. (2015). Degradable polyethylene: Fantasy or reality. *Environmental Science & Technology*, 49(7), 4218-4228. https://doi.org/10.1021/acs.est.5b00263

Sastri, V. R. (2021). *Plastics in medical devices: Properties, requirements, and applications* (3rd ed.). William Andrew.

Scheibe, B., Borowiak-Palen, E., & Kalenczuk, R. J. (2014). Oxidation and thermal stability of multiwall carbon nanotubes. *Journal of Thermal Analysis and Calorimetry*, 116(1), 273-279. https://doi.org/10.1007/s10973-013-3540-2

Schimazu Corporation. (2021). *FTIR spectrometer user manual*. Schimazu Scientific Instruments.

Skeist, I. (1966). *Plastics in building: An encyclopedia of architectural and construction applications*. Reinhold.

Smith, J., Johnson, L., & Brown, R. (2020). Thermal analysis of biodegradable polymers using differential scanning calorimetry. *Journal of Polymer Science*, 58(12), 1723-1735. https://doi.org/10.1002/pol.20200123

Stauber, R. (2007). *Automotive plastics and composites: Materials and processing*. William Andrew.

Szeteiova, K. (2010). *Automotive materials: Plastics in automotive markets today*. Smithers Rapra.

Torres, F. G., Troncoso, O. P., & Diaz, D. A. (2019). Biodegradability and mechanical properties of starch films from Andean crops. *International Journal of Biological Macromolecules*, 124, 1021-1027. https://doi.org/10.1016/j.ijbiomac.2018.11.292

Venugopal, V. (2021). *Marine polysaccharides: Food applications*. CRC Press.

Verma, D., Gope, P. C., & Maheshwari, M. K. (2018). *Lignocellulosic polymer composites: Processing, characterization, and properties*. Wiley.

Vinod, A., Sanjay, M. R., & Suchart, S. (2020). Renewable and sustainable biobased materials: An assessment on biofibers, biofilms, biopolymers and biocomposites. *Journal of Cleaner Production*, 258, 120978. https://doi.org/10.1016/j.jclepro.2020.120978

Wang, J., Gardner, D. J., & Stark, N. M. (2021). Moisture and oxygen barrier properties of cellulose nanomaterial-based films. *ACS Sustainable Chemistry & Engineering*, 9(1), 49-66. https://doi.org/10.1021/acssuschemeng.0c07305

Wu, Q. (2014). *Chitin and chitosan for regenerative medicine*. Springer